Electronic Supplementary Material (ESI) for Soft Matter.

Supplementary Material

Insoluble Layer Deposition and Dilatational Rheology at a Microscale Spherical Cap Interface

Anthony P. Kotula and Shelley L. Anna

Center for Complex Fluids Engineering, Carnegie Mellon University, Pittsburgh, PA

Glass capillary treatment

A glass capillary (TW100-6 Kwik-Fil borosilicate, World Precision Instruments) is connected to a pressure transducer and hydrostatic pressure column, which is used to generate a bubble at the capillary tip and measure the pressure inside the capillary. The capillary is tapered using a micropipette puller (MicroData Instrument Inc., PMP-102) so that one end of the capillary has an inner radius ranging from 30 – 50 μm. The glass capillary is acid washed, then the inside is treated with a hydrophobic coating (Dynasylan SivoCLEAR, Evonik) to promote contact line pinning at the glass-air-aqueous interface. The hydrophobic coating is flowed through the capillary, and then the capillary is rinsed using acetone and DI water. The glass capillary is placed in a 60°C oven for 15-30 minutes to dry before use.

Fluid exchange system

The system used to exchange fluid in the microtensiometer sample cell is shown as Region G in Figure 1 of the main text. The inlet port is connected to flexible tubing in a peristaltic pump (Cole-Parmer, Model #7553-30) by PTFE tubing. PTFE tubing is also used to connect the flexible tubing to the fluid reservoir (PYREX 1000 mL), and to connect to the waste container (PYREX 1000 mL). The inlet and outlet tubing connections are made using polyether ether ketone (PEEK) fittings connected to threaded holes machined in the device. When the pump is operating, the fluid in the sample cell is replaced with the reservoir fluid at a controlled volumetric flow rate between 0.2 – 0.72 mL/min.

Unshifted compression isotherms of DMPC and PA

Figure A1 shows measurements of the surface pressure versus the surface area of the spherical cap interface during steady compression experiments for DMPC at the air-water interface. For all initial surface pressures, the surface pressure increases as the surface area decreases. The compression rate for each curve is between 1×10^{-3} and 3×10^{-3} s^{-1} for all runs shown, and there is no strong dependence on the rate of compression over a range of 10^{-4} to 10^{-2} s^{-1}. The maximum increase in the surface pressure over the available surface area range increases with the initial surface pressure. For example, a DMPC interface corresponding to an initial surface pressure of 2.33 ± 0.47 mN/m achieves an increase in surface pressure of approximately 12 mN/m over the surface area range examined (to a maximum surface pressure of 14.75 ± 0.44 mN/m), but an interface starting at a greater initial surface pressure of 27.41 ± 0.35 mN/m achieves an increase in surface pressure of approximately 21 mN/m. At the two largest initial surface pressures, the measured datasets intersect at a surface area of approximately 5600 μm^2 and a surface pressure of approximately 35 mN/m. The interface compressed from an initial surface pressure of 24.75 ± 0.35 mN/m increases to a larger final surface pressure of 52.28 ± 0.29 mN/m compared with the measurement performed with an initial surface pressure of 27.41 ± 0.35 mN/m. The surface pressure of approximately 35 mN/m where the two datasets overlap has been noted previously in Langmuir trough experiments for DMPC where either a collapse of the interface[1] or a liquid condensed-solid phase transition[2] is observed.

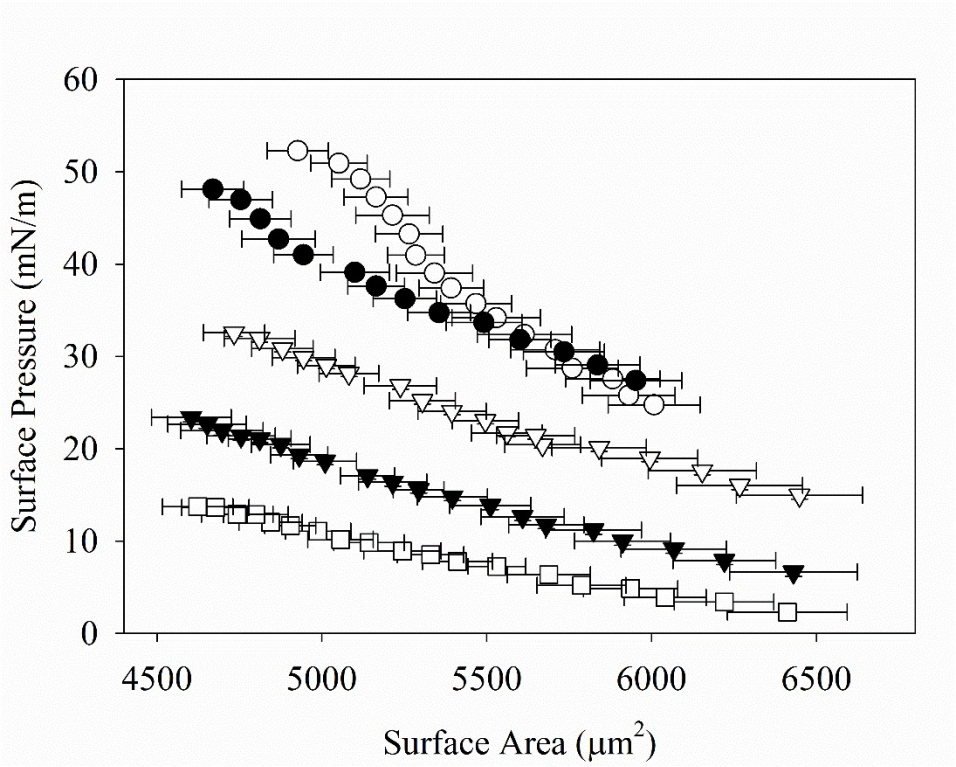

Figure A1. Surface pressure of DMPC as a function of the surface area of the spherical cap interface during a steady rate of inner pressure decrease at different initial surface pressures of 2.33 ± 0.47 mN/m (●), 6.64 ± 0.47 mN/m (▼), 14.95 ± 0.41 mN/m (♦), 24.75 ± 0.35 mN/m (▽), and 27.41 ± 0.35 mN/m (□).

Results from steady compression experiments for an interface with adsorbed PA are shown in Figure A2. The surface pressure-area response of the interface depends on the rate at which the hydrostatic pressure decreases. Over the range of hydrostatic pressure decrease rates considered here (1 to 100 Pa/s), the compression rate varies over roughly two orders of magnitude from $2 \times 10^{-4}\ s^{-1}$ at the smallest pressure decrease rate to $1 \times 10^{-2}\ s^{-1}$ at the largest pressure decrease rate. Although the surface pressure generally increases as the surface area decreases, the magnitude of the increase in surface pressure varies with initial surface pressure as well as dilatation rate. This can be seen from a comparison of the surface pressures for the interface compressed at a rate of $2 \times 10^{-4}\ s^{-1}$ from an initial surface pressure of 8.69 ± 0.44 mN/m

versus the interface compressed at $1 \times 10^{-2}\ s^{-1}$ with an initial surface pressure of 9.77 ± 0.45 mN/m in Figure A2. The interface compressed at $2 \times 10^{-4}\ s^{-1}$ achieves a final surface pressure of 16.65 ± 0.43 mN/m at a surface area of 4900 μm^2, but the interface compressed at $1 \times 10^{-2}\ s^{-1}$ increases to a maximum surface pressure of 55.75 ± 0.28 mN/m at a comparable surface area. The deviation in the isotherms compressed from 8.69 ± 0.44 mN/m and 9.77 ± 0.45 mN/m occurs at a surface pressure of approximately 10 mN/m, which is slightly greater than the equilibrium spreading pressure (9.7 mN/m).

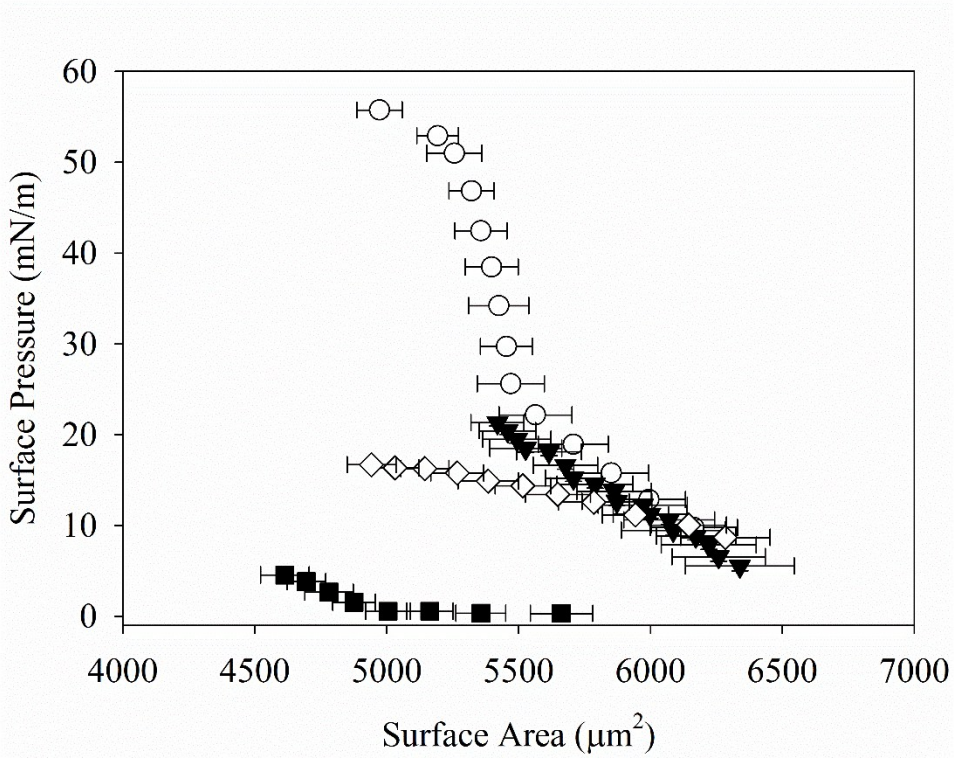

Figure A2. Surface pressure of PA versus the surface area of the spherical cap interface. The initial surface pressures and initial compression rates are 0.32 ± 0.49 mN/m and $3 \times 10^{-3}\ s^{-1}$ (○), 5.53 ± 0.50 mN/m and $3 \times 10^{-3}\ s^{-1}$ (▼), 8.69 ± 0.44 mN/m and $2 \times 10^{-4}\ s^{-1}$ (❋), and 9.77 ± 0.45 mN/m and $1 \times 10^{-2}\ s^{-1}$.

Dilatational modulus of DMPC and PA

The dilatational modulus of DMPC as a function of frequency is shown for four different surface pressures in Figure A3. The magnitude of the dilatational modulus is largely independent of frequency over the surface pressure range probed (2 mN/m < Π < 30 mN/m). At a surface pressure of 7.43 ± 0.49 mN/m, the magnitude of the dilatational modulus has an average value of $|E^*|$ = 65.6 ± 1.7 mN/m over the frequency range considered. The phase angle is on the order of 0.1 rad over the same frequency range, and decreases as the oscillation frequency increases. At a surface pressure of 13.58 ± 0.42 mN/m the average magnitude of the modulus is $|E^*|$ = 79.3 ± 2.0 mN/m, and the phase angle is less than 0.1 rad at low oscillation frequencies and decreases to a negligible value as the oscillation frequency increases. The average value of the modulus increases at a surface pressure of 25.88 ± 0.37 mN/m to 96.5 ± 3.0 mN/m. However, at a greater surface pressure of 30.35 ± 0.36 mN/m the average modulus decreases to 88.1 ± 2.6 mN/m. The phase angle decreases with frequency for Π = 25.88 ± 0.37 mN/m. Also, the phase angle remains at values less than 0.1 rad over the frequency range considered for all four surface pressures, indicating that the out-of-phase component of the modulus is too small to measure reliably for DMPC in these experiments. The phase angle increases with oscillation frequency at a surface pressure of 30.4 mN/m until the oscillation frequency reaches approximately 3.5 rad/s, after which the phase angle decreases to a negligible value.

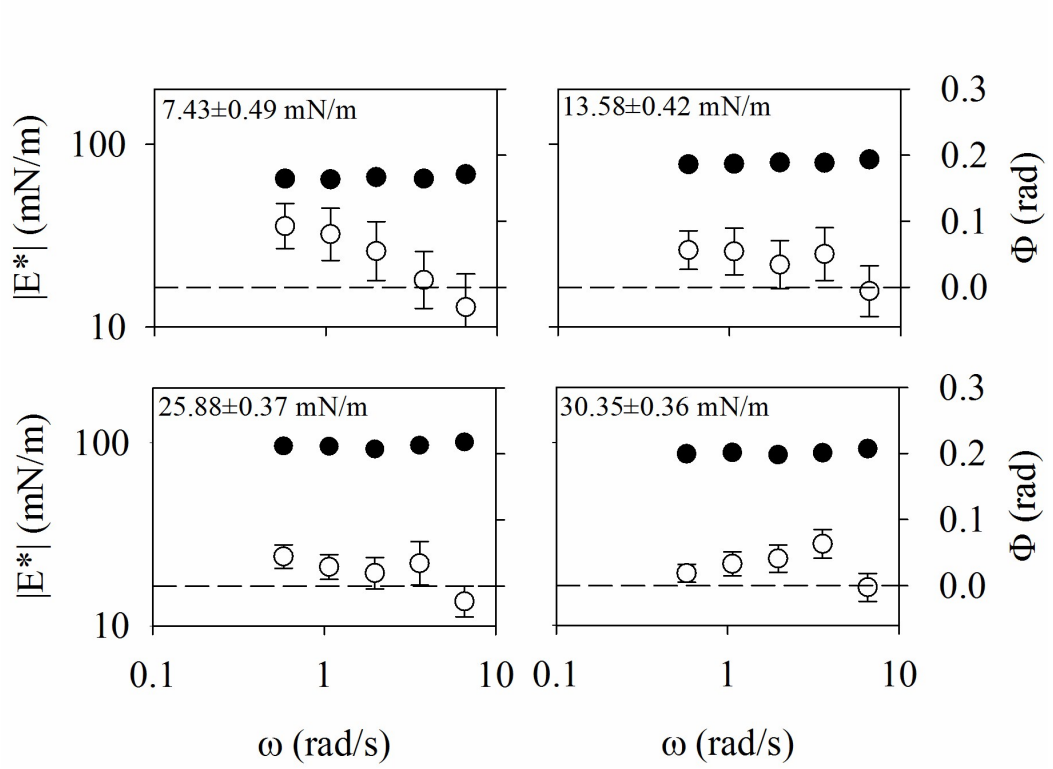

Figure A3. Dilatational modulus of DMPC versus angular frequency ω at surface pressures indicated in the upper left corner of each plot. The magnitude of the modulus $|E^*|$ (ꝏ) is plotted on the left axis and the phase angle Φ (ᘓ) is plotted on the right axis. The dashed line indicates the zero value for the phase angle in each plot.

Figure A4 shows the dilatational modulus measured for PA at surface pressures ranging from 1.35 ± 0.49 mN/m to 9.52 ± 0.42 mN/m. When the interface is dilated to surface pressures greater than 9.7 mN/m, the surface pressure and surface area both decrease over the time period of the oscillatory experiment (approximately 5 minutes). For example, after compression to an initial surface pressure of approximately 15 mN/m, the surface pressure decreases by 2 mN/m and the surface area decreases by 70 μm^2 over a period of one minute. The large variation in the size of the error bars indicates variability in the resolution of the bubble oscillation amplitude imposed by the oscillating hydrostatic pressure head.

For the four dilatational measurements shown in Figure A4, the magnitude of the modulus strongly depends on the surface pressure at which oscillation occurs. At a surface pressure of 1.35 ± 0.49 mN/m the dilatational modulus $|E^*|$ is approximately independent of

oscillation frequency with an average value of 35.2 ± 5.7 mN/m, and the phase angle has a maximum value of approximately 0.4 rad at an oscillation frequency of 1 rad/s. Dilatational measurements at a surface pressure of 3.01 ± 0.48 mN/m show an increase in the modulus with frequency from $|E^*| = 55.0 \pm 1.0$ mN/m at $\omega = 0.58$ rad/s to $|E^*| = 88.5 \pm 2.4$ mN/m at the largest frequency of $\omega = 6.57$ rad/s. At a surface pressure $\Pi = 5.82 \pm 0.50$ mN/m the dilatational modulus increases from 168.1 ± 6.1 mN/m to 242 ± 24 mN/m over the frequency range considered while the phase angle is negligible. At the highest surface pressure of 9.52 ± 0.42 mN/m, the modulus remains roughly constant with frequency at an average value of $|E^*| = 197 \pm 34$ mN/m while the phase angle decreases with oscillation frequency to negative values. Negative values are outside the physically sensible phase angle range of $0 \text{ rad} < \Phi < \pi/2 \text{ rad}$ for interfaces perturbed from an equilibrium state.[3] Comparing the dilatational modulus over the surface pressure range shown in Figure A4, the magnitude of the modulus increases as surface pressure increases. A phase angle less than zero corresponds to a negative value for the out of phase component of the modulus E'', which has been observed previously in dilatational measurements for PA monolayers performed on a Langmuir trough.[4]

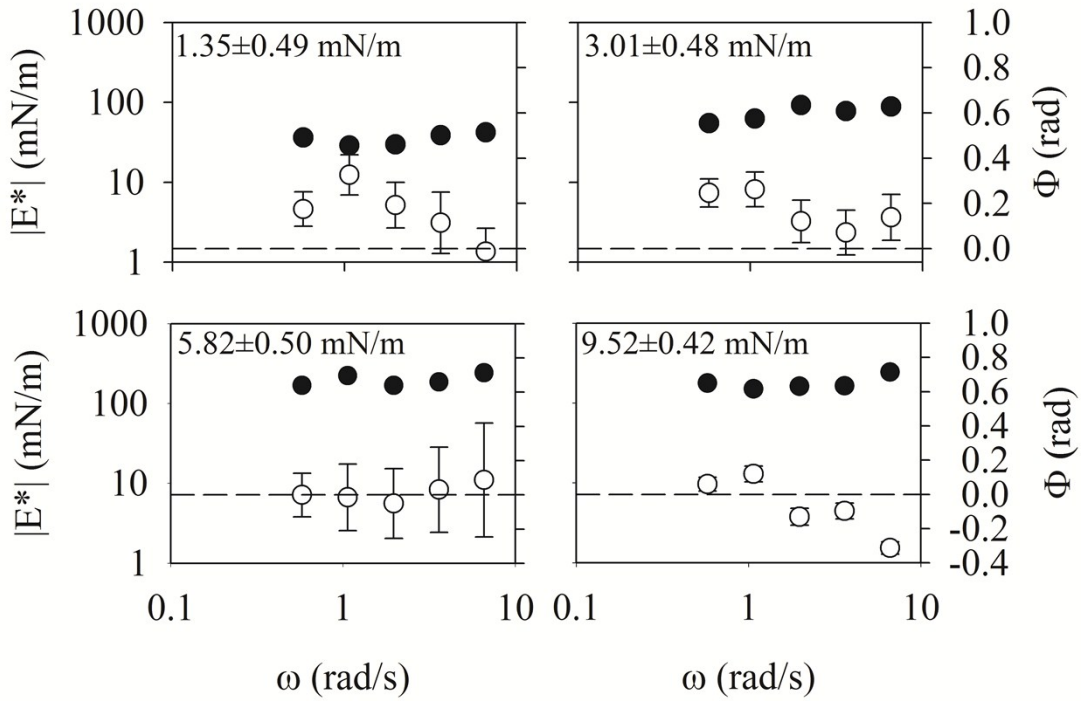

Figure A4. Dilatational modulus of PA versus angular frequency ω at surface pressures indicated in the upper left of each plot. The modulus $|E^*|$ (ℰ) is plotted on the left axis and the phase angle Φ (ℛ) is plotted on the right axis. The dashed line indicates the zero value for the phase angle in each plot.

Tween 80 dynamic surface tension, unshifted compression isotherm, and dilatational modulus

The dynamic surface tension of an air-water interface during the adsorption of Tween 80 and the subsequent exchange with DI water is shown in Figure A5. The initial transient for all curves is similar beginning with the generation of a clean interface at time t=0 until the initiation of the fluid exchange process at a later time (typically for t > 100 s). During the exchange process, the bulk concentration of Tween 80 is reduced from 1.5 μM to approximately zero over a time period of 300 s (more than 40 residence times). Complete rinsing is confirmed by generating a fresh air bubble after solvent exchange has occurred and observing that there is no change in the surface tension over a period of 1000 s. Consistent with the work of Reichert and Walker,[5,6] solvent exchange does not cause the surface tension to fully return to the clean air-water value of 72.8 mN/m as expected for reversibly adsorbed surfactants. Instead, the surface

tension rises to a smaller steady state value or remains constant after rinsing begins, indicating that all or a portion of the initially deposited material is irreversibly adsorbed.

The dynamic surface tension immediately following solvent exchange depends on the surface tension at the time that solvent exchange began. When the solvent exchange procedure is initiated at instantaneous surface tension values near 67 – 70 mN/m, the surface tension decreases by approximately 2 mN/m within approximately 10 s after the solvent exchange procedure is initiated. This decrease in the surface tension is attributed to increased mass transport at early time in the exchange period due to increased convection in the reservoir, which enhances the mass transfer rate of surfactant to the interface. The surface tension reaches a constant value approximately 40 s after the initiation of the exchange period. When the solvent exchange procedure is initiated at low instantaneous surface tension values near 52 mN/m, the surface tension rises to a constant value that is less than the clean air-water surface tension value. These results agree well with the observations of Reichert and Walker.[5, 6] The nonzero value of the surface pressure for these interfaces indicates that Tween 80 remains at the air-water interface to form an irreversibly adsorbed layer.

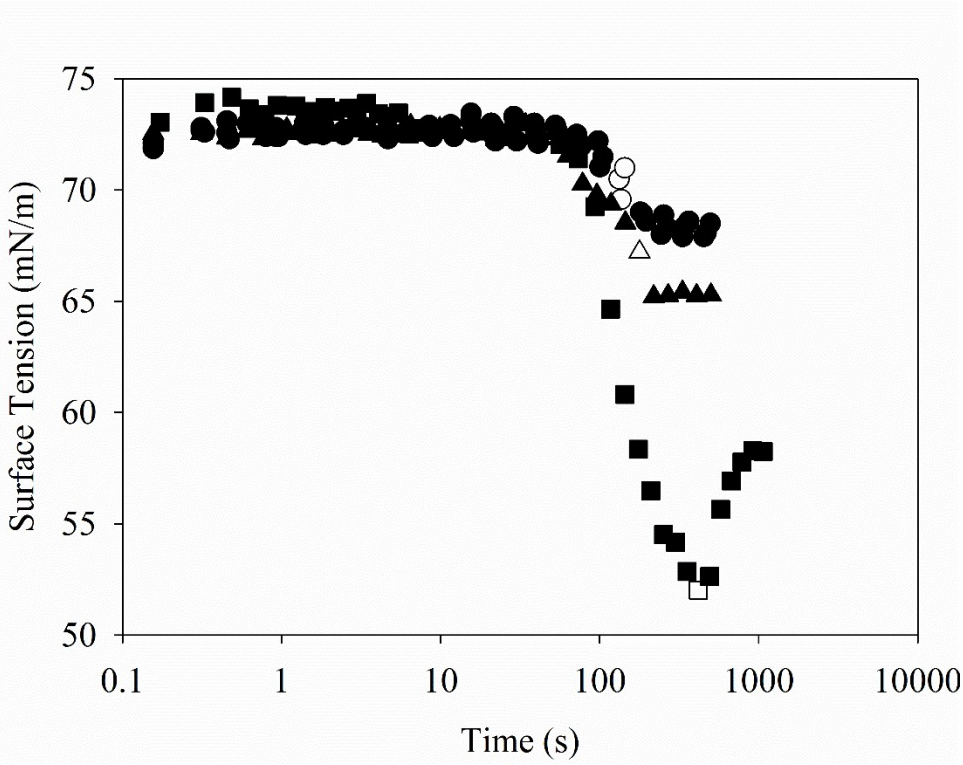

Figure A5. Dynamic surface tension for an air-water interface in contact with a 1.5 μM Tween 80 solution. The initial transient corresponds to surfactant adsorption and the late time transient corresponds to the solvent exchange. The final surface pressure at the end of the solvent exchange procedure is 4 mN/m (●) , 7.5 mN/m (▲), and 14.5 mN/m (■). The open symbol in each curve indicates the time at which the solvent exchange procedure begins. Three measurements corresponding to a final surface pressure of 4 mN/m are shown to indicate reproducibility.

Figure A6 shows the surface pressure measured during quasi-steady compression for four separate irreversibly adsorbed Tween 80 interfaces with no excess surfactant present in the aqueous phase. Each interface is compressed at a constant rate of decrease in hydrostatic pressure head of 10 Pa/s, leading to an average dilatation rate of the interface of $1\times10^{-3} < \dot{\delta} < 3\times10^{-3}$ s^{-1}. The surface pressure-area isotherms for the irreversibly adsorbed Tween 80 interface are independent of the hydrostatic pressure decrease rate (and therefore the compression rate) over the experimentally accessible range. All four surface pressure-area measurements for the insoluble component of Tween 80 at an air-DI water interface exhibit an increase in the surface pressure as the surface area decreases. The total change in the surface pressure over the surface area range probed is approximately 3 mN/m for each curve and is

independent of the initial surface pressure. A plateau is observed at a surface pressure of 17 mN/m for the Tween 80 interface dilated from an initial surface pressure of 13.43 ± 0.42 mN/m, which is the maximum surface pressure value we attain for the interfaces generated from the solvent exchange experiments shown in Figure A5.

The presence of Tween 80 in oil-water emulsions is observed to influence the measured zeta potential of the oil droplets,[7-9] suggesting that there is an accumulation of charge at the interface due to the surfactant. To test whether charge accumulation has a significant effect on the surface pressure isotherm, compression experiments were performed on interfaces for which the DI water subphase is exchanged with a 0.5 M NaCl solution to screen any charge effects. The compression isotherms shown in Figure A6 for a 0.5 M NaCl solution subphase show no significant deviation from the isotherms obtained for a DI water subphase at comparable initial surface pressures.

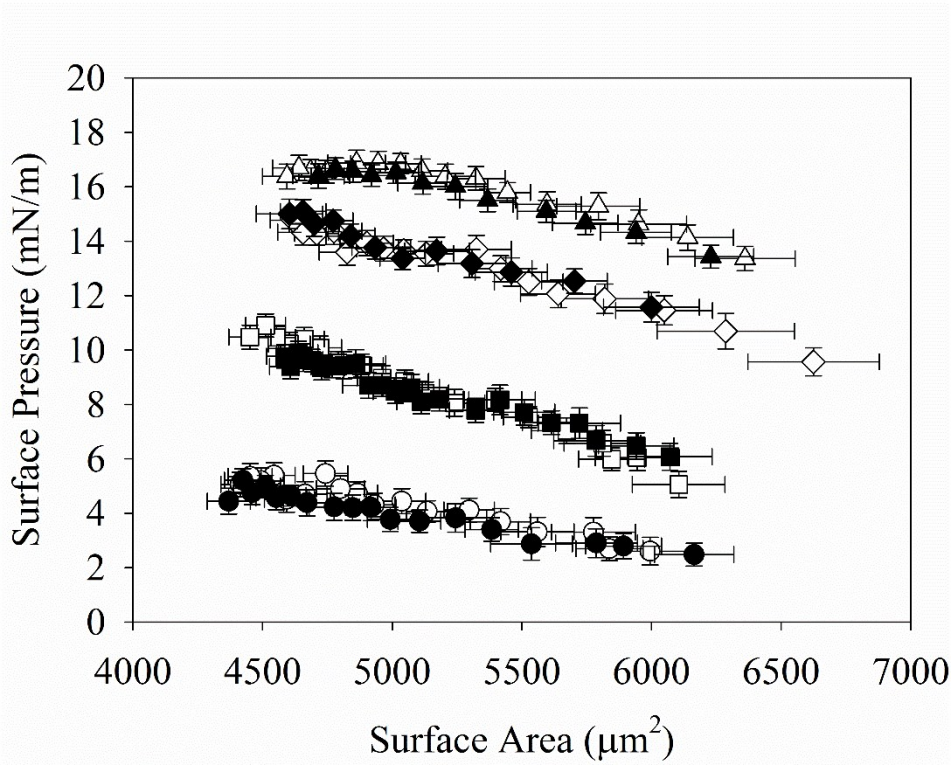

Figure A6. Compression measurements for the insoluble component of Tween 80 at an air-water interface. Surface pressure versus the surface area of the spherical cap bubble at initial surface pressures of 2.48 ± 0.42 mN/m (ᘐ), 2.61 ± 0.50 mN/m (ᘓ), 5.06 ± 0.48 mN/m (●), 6.08 ± 0.50 mN/m (○), 9.57 ± 0.52 mN/m (❋), 11.57 ± 0.54 mN/m (✹), 13.37 ± 0.45 mN/m (❒), and 13.43 ± 0.42 mN/m (□). Open symbols correspond to measurements in contact with a 0.5 M NaCl solution subphase, and filled symbols were performed with a DI water subphase.

Representative measurements of the dilatational modulus performed for irreversibly adsorbed layers of Tween 80 are shown in Figure A7. The dilatational modulus is independent of frequency over the surface pressure range of approximately 2 mN/m < Π < 17 mN/m. The phase angle is too small to be resolved in these experiments, indicating that the out of phase component of the modulus E'' is negligible. The average magnitude of the modulus over the frequency range considered for an irreversibly adsorbed Tween 80 interface in contact with a DI water subphase is $|E^*| = 23.1 \pm 3.8$ mN/m at a surface pressure of 6.44 ± 0.48 mN/m. For an insoluble Tween 80 interface with higher surface pressure of Π = 13.21 ± 0.47 mN/m in contact with a

0.5 M NaCl subphase, the average modulus is 19.4 ± 2.0 mN/m. It is important to note that the dilatational modulus data presented here correspond to two insoluble Tween 80 interfaces generated through independent fluid exchange procedures, as opposed to the same interface probed at a different surface pressure or subphase composition. The dilatational response of an irreversibly adsorbed Tween 80 interface is different from the average dilatational modulus measured on fatty acid layers such as PA, which increases significantly with increasing surface pressure, as shown in Figure A4. The lack of frequency dependence of the in phase component of the modulus E' and a negligible phase angle Φ is consistent with an interface whose mechanics are determined solely by surface tension changes.

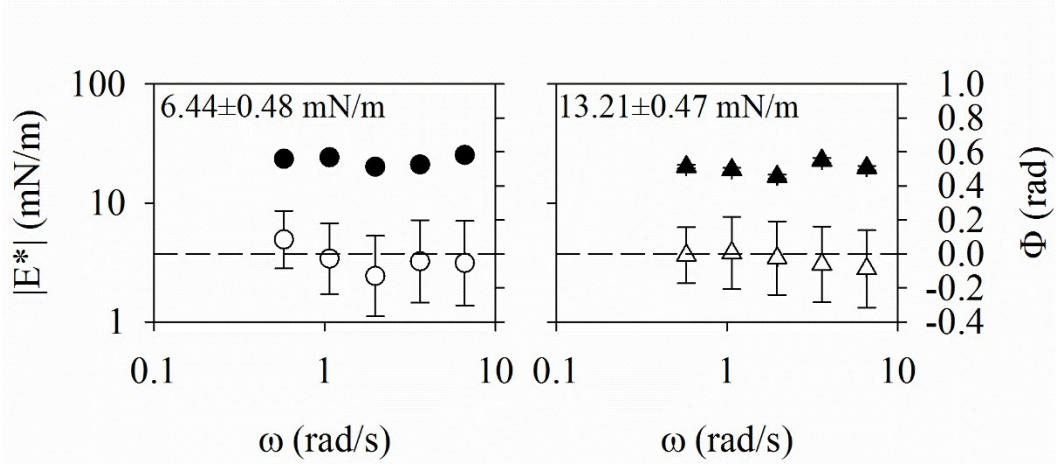

Figure A7. Dilatational modulus of Tween 80 versus angular frequency ω at surface pressures indicated in the upper left corner of each plot. The modulus $|E^*|$ (℘,□) is plotted on the left axis and the phase angle Φ (ᖇ,❒) is plotted on the right axis. The left plot is measured on a DI water subphase, and the right plot is measured on a 0.5 M NaCl subphase. The dashed line indicates the zero value for the phase angle in each plot.

References

1. I. Kubo, S. Adachi, H. Maeda and A. Seki, *Thin Solid Films*, 2001, **393**, 80-85.
2. M. Li, U. Retter and J. Lipkowski, *Langmuir*, 2005, **21**, 4356-4361.
3. A. P. Kotula and S. L. Anna, *Journal of Rheology*, 2014, **59**.
4. J. Giermanska-Kahn, F. Monroy and D. Langevin, *Physical Review E*, 1999, **60**, 7163.
5. M. D. Reichert and L. M. Walker, *Langmuir*, 2013, **29**, 1857-1867.
6. M. D. Reichert, Ph.D. Dissertation, Carnegie Mellon University, 2013.
7. J.-P. Hsu and A. Nacu, *Journal of Colloid and Interface Science*, 2003, **259**, 374-381.

8. G. Stalidis, A. Avranas and D. Jannakoudakis, *Journal of Colloid and Interface Science*, 1990, **135**, 313-324.
9. A. Avranas and G. Stalidis, *Journal of Colloid and Interface Science*, 1991, **143**, 180-187.